Impact of a partly sealed fault on hydro-mechanical properties of a granite reservoir

EGU2020-15484

Guido Blöcher[1,2], Christian Kluge[1], Mauro Cacace[1], Harald Milsch[1], Jean Schmittbuhl[2]

[1] GFZ German Research Centre for Geosciences, Potsdam, Germany
[2] EOST-IPGS, Université de Strasbourg/CNRS, Strasbourg, France

Abstract

The fluid flow in Enhanced Geothermal Systems (EGS) is dominated by hydraulically stimulated fractures and faults which are the key elements of their hydraulic performance and sustainability. At the fault scale, the flow performance is influenced by the aperture distribution which is strongly dependent on the fault roughness, the geological fault sealing, the relative shear displacement, and the amount of flow exchange between the matrix and the fault itself. On the mechanical side, stiffness and strength of partly sealed fault might alter or reinforced the mechanical behavior of the fault zone in particular with respect to new stimulations. In order to quantify the impact of chemical soft stimulation in EGS reservoir on the hydro-mechanical properties of a fault-rock system that includes fault-filling material, we conducted numerical flow through experiments of a granite reservoir hosting one single partly sealed fault of size 512x512 m^2. In order to mimic the chemical alteration of the fault-rock system we sequentially changed the distribution pattern of the fault-filling material by means of a hydro-poro-elastic coupled simulation. Navier-Stokes flow is solved in the 3-dimensional rough aperture and Darcy flow in the related poro-elastic matrix. By means of this model, an evaluation of the local channeling effect through the fault for various degrees of sealing was performed. Based on the obtained results, we derived a macroscopic change of the hydraulic-mechanical behavior of the fault-rock system, e.g. permeability change, fracture stiffness modulus.

Fault Aperture

Faults are typically considered as two dimensional objects, their thickness being often neglected in front of the extension. They are then approximated as planar surfaces. However, even as 2D objects, they show multi-scale corrugations that can be interpreted as a self-affine roughness over a very large range of scales (up to 9 decades of length scales). They even exhibit a possible anisotropy owing to the fault slip direction (Candela et al., 2012). It was evidenced that the roughness exponent was of the order of $H_{//} = 0.6$ along the slip direction and $H_{perp} = 0.8$ in the perpendicular direction. Here we considered a synthetic 512 m x 512 m fault that reproduces this geometry over the range of scales accessible in the model (see Fig. 1a where the scaling of the power spectral density is shown for a large collection of natural faults together with that of our synthetic fault surface). From this fault topography, we assessed the fault aperture assuming that the cumulative fault offset is large compared to the size of the fault domain we are considering. In doing so, the fault aperture is made of the facing of two independent fault surfaces and subsequently have the scaling properties of one of this surface. Accordingly, we generated the fault aperture as an anisotropic self-affine surface with $H_{//} = 0.6$ along the slip direction (y-axis) and $H_{perp} = 0.8$ along the perpendicular direction (x-axis) and a RMS amplitude of 0.1 m at the 512 m scale (see Fig. 1b). Fig. 1c is showing the histogram of the aperture distribution in the whole fault domain of 512 m x 512 m which is well approximated by a gaussian distribution.

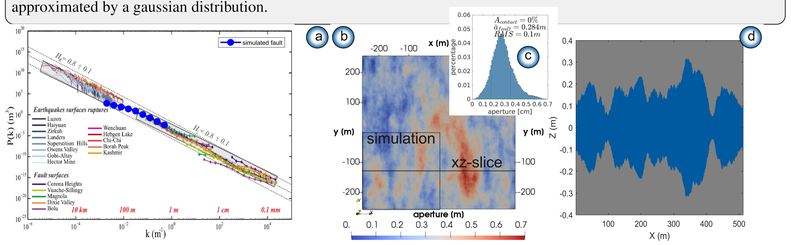

Figure 1: Generation of fault topology and aperture map: (a) power spectral density; (b) aperture map including simulation domain; (c) histogram of aperture distribution; and (d) xz-slice through the rock-fault with a vertical magnification of approximately 600.

Mesh Generation

The synthetic fault topology and aperture map were used as an input structure for finite element mesh generation. The input structure is a regular grid with a grid spacing of 1 m, a dimension of 512 m by 512 m, and a minimum aperture of 0 m. For the mesh generation a spacing of 4 m and a dimension of 256 m by 256 m were chosen. Considering a mean aperture of approximately 0.25 m, the fault aspect ration is 1:1000. In order to mimic the precipitation of filling material in the fault (considered as coating) we interpenetrate the two surfaces of the fault stepwise from 0.059 m (c0) to 0.199 m (c7). Which results in a contact area between 14.3 % and 65 % for c0 and c7, respectively. Such an interpenetration leads to sharp edges between the two surfaces, which subsequently will lead the a huge amount of tetrahedral elements. To overcome this limitation we truncated all fault apertures below 0.1 m, resulting in a minimum fault aperture of 0.1 m for all cases.

To represent the fault (aspect ratio 1:1000) by a useful amount of tetrahedral elements (Fig. 2a) we used an anisotropic mesh (Fig. 2b). Normal to the fracture surface we used a discretization of 3 element layers at the fault tip and 5 elements layers at the wider part of the fault. Along the fracture we introduced elements having an aspect ratio of 1:25. Therefore the minimum element size normal and parallel to the fault is 0.033 m and 0.83 m, respectively. For meshing the rock we used an isotropic mesh with an element size of 0.83 m close to the fault. The element size is coarsening with increasing distance to the fault. The tetrahedralization was performed by using Gmsh (C. Geuzaine & J.-F. Remacle, 2009), a 3-D finite element mesh generator.

The amount of elements is varying for the individual cases. For the fault we generated between 185.000 and 730.000 tetrahedral elements for c7 and c0, respectively. For the rock, we generated between 1.886.000 and 2.213.000 tetrahedral elements for c0 and c7, respectively.

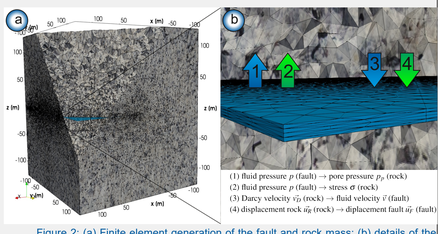

Figure 2: (a) Finite element generation of the fault and rock mass; (b) details of the transfer functions at the fault-rock interface.

Numerical Method

To analyse the stress, pressure and velocity field in a fault-rock system, an adequate physical model of the involved processes and their coupling is required. The Multiphysics Object Oriented Simulation Environment (MOOSE) in combination with GOLEM (Cacace & Jacquey, 2017), a MOOSE-based application for modelling coupled Thermal-Hydraulic-Mechanical (THM) processes in fractured and faulted geothermal reservoirs were used. To represent the rock matrix, we considered a poroelastic behaviour as implemented in Cacace & Jacquey (2017). For the fluid phase, the incompressible Navier-Stokes flow is implemented (Peterson, 2018). The Navier-Stokes module solves for the pressure and the velocity field inside the fault only. For the rock matrix, the primary variables solved for are pore pressure and displacement. The fluid velocity in the porous matrix as well as the strain and stress field are derived from these primary quantities. To derive a coupling between the two physical systems, i.e. the open fault and the rock domain, four exchange functions along the interfaces (Fig. 2b) between the rock and the fault were defined. Since the fluid pressure inside the fault is solved almost instantaneously when compared to the time scale of pore pressure diffusion in the rock, we used this pressure as boundary condition for the pore pressure in the rock matrix system (see (1) in Fig. 2b). Furthermore, this pressure acts as a body force on the rock matrix. Therefore, we used the pressure as a stress boundary condition in the rock matrix system (see (2) in Fig. 2b). Based on this pore pressure we calculated the fluid velocity in the rock domain following Darcy's law. This fluid velocity was assigned as a slipping boundary for the fracture flow inside the fault (see (3) in Fig. 2b). To impose the mechanical coupling and the corresponding deformation of the fault, the displacement values obtained in the rock matrix were assigned as boundary for the fault surface (see (4) in Fig. 2b). Since the incompressible Navier-Stokes flow does not consider the solid displacement as a primary variable, we used the displacement vector field to geometrically alter the fault mesh at each time step resulting in a displaced mesh configuration that will update the final solution for the dynamic pressure and fluid velocity field.

In order to derive a solution for the fault-rock system, the following initial and boundary conditions were chosen. The initial condition for the rock matrix is: pore pressure and displacement field equal to zero. Furthermore, the fluid pressure and the velocity inside the fault are set to zero. In addition to the boundary conditions applied at the interface, we imposed a flow either in x or y direction by setting an inlet pressure to 10 Pa. At the outlet, we kept the pressure constant at zero during the total transient simulation. At all other side walls of the fault and rock we imposed a no flow boundary by setting the velocity vector to zero. For the mechanical part we set a zero displacement in z-direction for the bottom and no displacement in x-y-direction for the lateral borders as well as for the inlet and outlet. At the top of the rock matrix system, i.e. along the z-direction, we applied a compressive stress gradually increasing from 0 to 1 MPa.

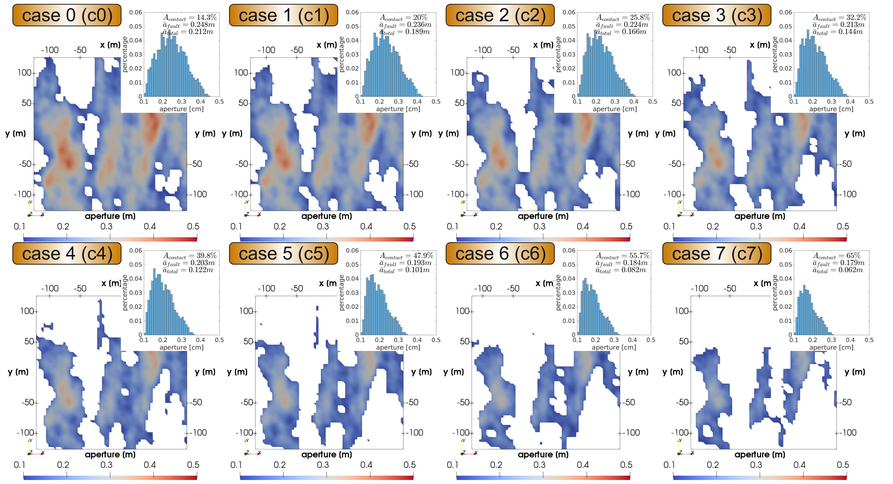

Figure 3: Aperture maps of the simulation cases 0 to 7 (c0 to c7) during the progressive steps of fault sealing including the related histograms of aperture distribution (inserts).

Method

The sealing of the fault is approximated by imposing a coating along the fault surfaces. All together 8 cases (c0, c1, … , c7) with increasing coating thickness were simulated. For each case we increased the coating thickness by 0.01 m, leading to a stepwise decrease in fault aperture of 0.02 m. For each of the 8 cases three hydraulic-mechanical coupled simulations were performed:

a) general flow along x-direction with a gradient of 10 Pa/256 m
b) general flow along y-direction with a gradient of 10 Pa/256 m
c) vertical load in z-direction with a loading rate of 0.1 MPa/h

For the scenarios (a) and (b) the permeability k_{total} of the overall system (fault + rock mass) was calculated. For scenario (c) we calculated the stiffness modulus K of the fault-rock system. The permeability of the overall system was calculated based on the constant pressure boundary at the inlet (matrix and fracture) and at the outlet. For the overall system the cross-sectional area A_{total} will not change and the total permeability can be obtained as follows:

$$\frac{\dot{V}}{A_{total}} = v = -\frac{k_{total}}{\mu}\nabla p. \quad (1)$$

In accordance to Pyrak-Nolte & Morris (2000), the specific fracture stiffess, κ, is equal to the change in stress divided by the change in displacement of the fracture:

$$\kappa = \frac{\Delta\sigma}{\Delta u}$$

Unfortunately, such a definition will not stand at the scale of the reservoir. Indeed, at reservoir scale a small change in vertical stress (1 MPa) will lead to a displacement in the range of 0.03 m and, henceforth, the effective pressure stiffness will be small in comparison to reported values. Therefore, we defined an effective fracture modulus K, similar to the Young's modulus, which relates the change in stress to the change in total strain:

$$K = \frac{\Delta\sigma}{\Delta\varepsilon}. \quad (2)$$

Results

Although only a pressure gradient of 10 Pa/256 m was applied, we determined a volume flux through the fault of 4.4 and 8.7 m^3/s along the x-direction and y-direction, respectively. The related calculated permeability for c0 is in the range of 2e-06 m^2. Due to a progressive sealing of the fault, we reached the percolation threshold when the flow is in the x-direction between c4 and c5 (Fig. 4h). This situation reduces the permeability of the overall system to 2.15e-16 m^2. In comparison the rock permeability is 2e-16 m^2. In contrast, the permeability in y-direction is only reduced from 3.4e-06 m^2 (c0) to 9.0e-8 m^2 (c7). The distribution of the velocity field in the fault-rock system indicates, that the total permeability is dominated by the flow in the fault. Due to a strong channeling effect a maximum velocity magnitude of 0.5 m/s was observed at critical bottlenecks of the fault (Fig. 4a,b,d,e). In contrast, the maximum velocity magnitude in the rock matrix is approximately 1e-13 m/s. Due to this low velocities in the rock matrix, it took almost 10 years to reach a steady state pressure (Fig. 4c,f) and velocity field in the rock domain.

Based on the applied stress of 1 MPa and the responding total strain, we calculated the stiffness modulus of the fault-rock system. The stiffness modulus is shown to be a linear function of the contact area along the fault zone. With increasing sealing of the fault (i.e. the fault volume is decreasing from 12.400 to 4.100 m^3), the stiffness modulus is increasing from 8 GPa to 18 GPa (Fig. 4i). It can be approximated, that the stiffness modulus is close to the Young's modulus of the rock mass for a contact area of 100 %. Besides the increase of the stiffness modulus, we observed a stress concentration at the asperities of the fault (Fig. 4g). The maximum stress concentrations were observed at the asperity boundaries. It is shown that the stress concentrations are the ratio of the applied stress at the top and the actual contact area along the fault. For c3 (Fig. 4g) having a contact area of 32.2 % the applied stress of 1 MPa turns into a stress concentration of 5 MPa at the asperity boundaries (red domains).

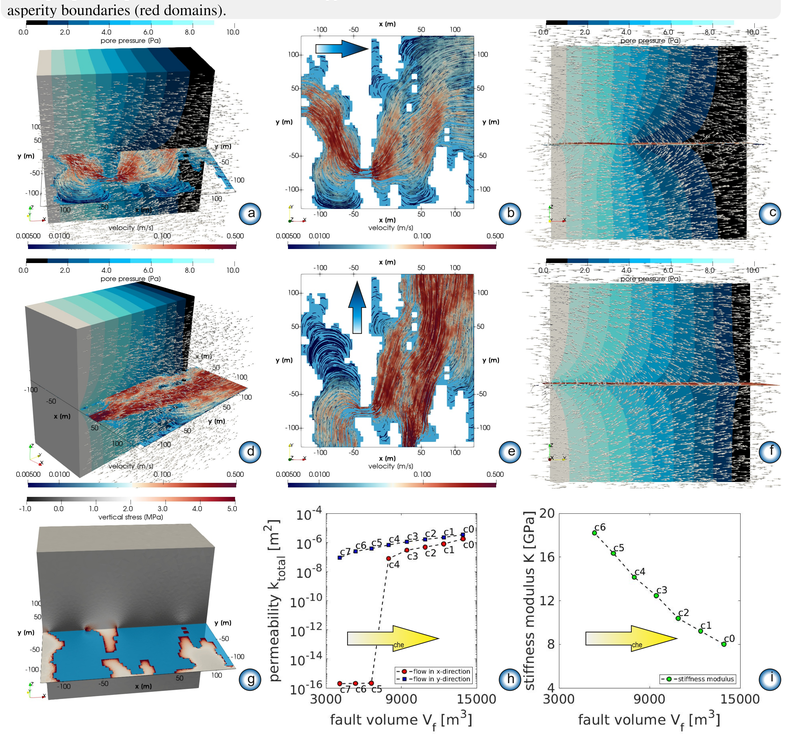

Figure 4: Simulation results: (a)-(c) pressure and velocity field for c3 with imposed flow in x-direction; (d)-(f) in y-direction; (g) vertical stress distribution for c3; (h) permeability evolution in x and y direction as function of the fault volume; and (i) stiffness modulus of the overall system.

Conclusions

By means of the presented fully 3-dimensional numerical approach, we simulated the hydraulic-mechanical behaviour of a partly sealed fault embedded in a granite reservoir. Here, faults with a aspect ratio of 1:1000 could be handled. The progressive sealing of the fault was simulated by adding stepwise a coating to the fault surfaces, which progressively reduces the fault aperture. At a certain degree of sealing we reached the percolation threshold with regards to the flow in x-direction (perpendicular to the slip direction). This results in a dramatic reduction of permeability by 9 orders of magnitude. In contrast, the permeability along the slip direction is almost constant (reduced by a factor of 2).

The success of a chemical treatment to increase the permeability of a partly sealed fault strongly depends on the degree of sealing. If flow paths are open in all directions, a chemical treatment will have minor impact. If anisotropic flow behaviour is observed (a directional percolation threshold exists), a chemical treatment could have major impact. To quantify the degree of sealing, the stiffness modulus of the fault can be used. The stiffness modulus of the fault is a function of contact area and, henceforth, a function of degree of sealing. If the stiffness modulus can be derived by field measurements, the degree of sealing can be estimated and the success of a chemical treatment can be evaluated. In summary, chemical treatments should be considered for faults-rock systems with high anisotropy in permeability and with high stiffness modulus close to the Young's modulus of the rock mass.

Acknowledgements

The authors are grateful for the funding received from the European Commission Horizon 2020 research and innovation programme under grant agreement No. 691728 (DESTRESS).

References

[1] Cacace, M. and Jacquey, A. B.: Flexible parallel implicit modelling of coupled thermal–hydraulic–mechanical processes in fractured rocks, Solid Earth, 8, 921–941, https://doi.org/10.5194/se-8-921-2017, 2017.

[2] Candela, T. and Renard, F. and Klinger, Y. and Mair, K. and Schmittbuhl, J. and Brodsky, E. E.: Roughness of fault surfaces over nine decades of length scales, Journal of Geophysical Research: Solid Earth, 117, B08409, doi:10.1029/2011JB009044, 2009.

[3] Geuzaine, C. and Remacle, J.-F.: Gmsh: A 3-D finite element mesh generator with built-in pre- and post-processing facilities, International Journal for Numerical Methods in Engineering, 79, 1309–1331, https://doi.org/10.1002/nme.2579, 2009.

[4] Peterson, J. W., Lindsay, A. D., and Kong, F.: Overview of the incompressible Navier–Stokes simulation capabilities in the MOOSE framework, Advances in Engineering Software, 119, 68–92, https://doi.org/10.1016/j.advengsoft.2018.02.004, 2018.

[5] Pyrak-Nolte, L. and Morris, J.: Single fractures under normal stress: The relation between fracture specific stiffness and fluid flow, International Journal of Rock Mechanics and Mining Sciences, 37, 245–262, https://doi.org/10.1016/s1365-1609(99)00104-5, 2000.